Orientational ortho-H_{2} pair interactions in the microporous framework MOF-5

Stephen A. FitzGerald, Christopher T. Eckdahl, Cooper S. McDonald, Jocienne N. Nelson, Kai Shinbrough, Holden W. H. Lai, and Jesse L. C. Rowsell

Phys. Rev. B **92**, 134304 — Published 9 October 2015

DOI: 10.1103/PhysRevB.92.134304

Orientational ortho-H_2 pair interactions in the microporous framework MOF-5

Stephen A. FitzGerald,[1,*] Christopher T. Eckdahl,[1] Cooper S. McDonald,[1] Jocienne N. Nelson,[1] Kai Shinbrough,[1] Holden W. H. Lai,[1,2] and Jesse L. C. Rowsell[2]

[1] *Oberlin College Physics and Astronomy*
[2] *Oberlin College Chemistry*

Infrared spectroscopy is used to observe the orientational fine structure arising from *ortho*-H_2 adsorbed at the primary site of the microporous framework MOF-5. The $Q_1(1)$ vibrational transition shows at least two symmetrically spaced fine structure bands on either side of the main band. These grow in relative intensity with increasing H_2 concentration indicative of interacting H_2 pairs. This interpretation is strongly supported by D_2 addition experiments, which cause a large increase in intensity of the fine structure bands with only minimal change in the main band. The spectra are analyzed in terms of $H_2 \cdots H_2$ electric quadrupole-quadrupole interactions. Consistent with this approach we observe no fine structure bands for the $Q_1(0)$ vibrational transition arising from *para*-H_2, which does not possess a quadrupole moment.

PACS numbers: 68.43.–h, 33.20.Ea, 33.15.Pw, 34.20.Gj

I. INTRODUCTION

Solid hydrogen is a molecular quantum crystal in which the individual molecules are almost freely rotating even at the lowest temperature[1,2]. This leads to a rich infrared (IR) behavior with extremely sharp lines[3–6]. In particular, solid *para* hydrogen, in which the nuclear spin quantum number I = 0 and the molecular rotational quantum number J = 0, is seen as an ideal matrix to study isolated impurity species[7]. In a J = 0 state, *para*-H_2 does not possess a quadrupole moment and its intermolecular interactions are purely isotropic. In contrast, *ortho*-H_2 (I=1, J = odd and = 1 at low temperature) has a quadrupole moment and significant anisotropic interactions. Much work has been devoted to the study of isolated pairs of *ortho*-H_2 within an otherwise *para* hydrogen solid[3,6,8–10]. Electric quadrupole-quadrupole (EQQ) interactions within *ortho*-H_2 pairs lift the orientational degeneracy leading to a complex IR spectrum[1,3,8]. This array of closely spaced IR lines that only became apparent with high-resolution spectroscopy have been referred to as the pair or alternatively, fine structure spectrum[6,9,10]. We will use the term fine structure (FS) throughout this paper.

In this investigation we extend the work with *ortho*-H_2 pairs by trapping small numbers of H_2 molecules at isolated sites within a metal-organic framework (MOF) crystal. MOFs are a class of materials consisting of metal coordination clusters joined together by organic linkers to form microporous structures[11–14]. Due to their high porosity and crystalline nature, MOFs have received much attention with regards to hydrogen storage. The MOF composition and structure can in principle be tuned to a particular purpose. However, to date no MOF has been achieved with the necessary properties to store H_2 under ambient conditions. In particular obtaining a material with the optimal H_2 adsorption enthalpy of -15 to -20 kJ/mol is seen as key[15]. MOF$\cdots$$H_2$ interactions arise from dispersion (van der Waals), polarization, and charge-transfer mechanisms[15]. These are notoriously difficult to model due to the inherent electron correlation terms and the complexity of the MOF unit cell[16]. Because the IR activity of H_2 trapped within a MOF arises from MOF$\cdots$$H_2$ interactions, their spectra provide an ideal way to test the different proposed interaction models. Additionally, IR features that arise through $H_2 \cdots H_2$ interactions should provide direct information about the state of the adsorbed H_2 and the degree to which charge-transfer and polarization has occurred.

MOF-5 is a prototypical framework with one of the largest hydrogen storage capacities by weight[17]. Neutron diffraction has provided the most descriptive experimental evidence of the preferred H_2 adsorption sites in this material[18,19]. There are four equivalent crystallographic positions referred to as the cup or primary site per MOF $Zn_4O(O_2C–)_6$ cluster. Below 50 K and concentrations of four H_2 per cluster, essentially all of the adsorbed H_2 are located at these primary sites[19]. At higher loadings less strongly bound sites become populated[18].

In addition to MOF-5 being the most well characterized of the MOFs, it also produces some of the sharpest IR spectra for an adsorbed species, making it an ideal test material[20,21]. In an earlier paper we measured the rovibrational IR spectrum for H_2 in MOF-5 that established the frequencies for the pure vibrational (Q), rotational sideband (S), and translational sideband (Q_{trans}) transitions[20]. These data were used by Kong et al. to theoretically model the interaction potential between the H_2 and the MOF[22], and more recently by Matanovic et al. using a quantum mechanical five-dimensional approach[23]. However, in neither of these models were $H_2 \cdots H_2$ interactions included. While $H_2 \cdots H_2$ interactions are well understood in the case of solid hydrogen[2] and isolated pairs of H_2 molecules[1], it is not clear how these interactions need to be modified in the case of adsorbed H_2. This will prove critical for any practical device aimed at hydrogen storage or isotopologue separation in which $H_2 \cdots H_2$ interactions need to be taken into account.

While earlier work hinted at FS associated with ad-

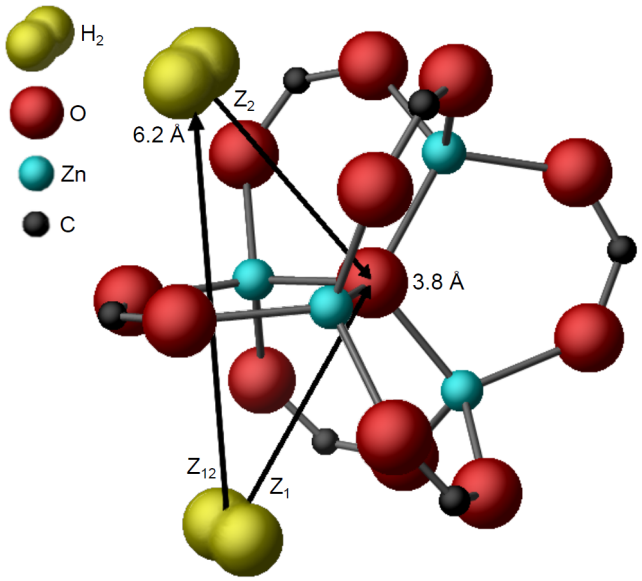

FIG. 1: (Color online) $Zn_4O(O_2C–)_6$ cluster showing two of the four possible primary sites occupied by H_2 molecules. The sites are separated by 6.2 Å and each has 3-fold symmetry about a Z-axis joining it to the central oxygen atom at a distance of 3.8 Å.

sorbed H_2 spectra, none used the necessary combination of low temperature, low H_2 concentration, and high resolution to resolve individual features[20,21,24]. In this paper we focus on conditions in which only the cup or primary site of MOF-5 is occupied with H_2. The next section provides a theoretical background to EQQ interactions, while the experimental data are presented in terms of H_2 concentration and time dependent spectra, along with the effects due to D_2 addition.

II. $H_2 \cdots H_2$ INTERACTIONS

Figure 1 shows MOF-5 with two of the four possible primary sites of a $Zn_4O(O_2C–)_6$ cluster occupied by adsorbed H_2 molecules. The sites are separated by 6.2 Å and arranged in a tetrahedron around the central oxygen atom[18,19]. There are also three next nearest-neighbor sites (not shown) on different MOF clusters at a distance of 8.6 Å[18,19].

In contrast to solid hydrogen, crystal field effects dominate the H_2 level splitting in MOF-5 with the interaction between pairs of H_2 molecules acting as a smaller perturbation. As shown in Fig. 2, crystal field effects cause the triply degenerate J = 1 state to both split and shift to lower energy. The m = 0 level (H_2 "pointing" towards the central oxygen atom) is now significantly higher in energy than either the m = ±1 levels[22]. We note that Ref.[22] uses two conflicting definitions for the these levels and so we adopt the ±1 form which we take be the more physical. In this notation the single particle states are defined as $|\pm\rangle = 1/\sqrt{2}\left(|m=1\rangle + |m=-1\rangle\right), |\mp\rangle = 1/\sqrt{2}\left(|m=1\rangle - |m=-1\rangle\right), |0\rangle = |m=0\rangle$. Defining a"crystal" Z_1-axis as that joining the H_2 to the central oxygen atom, Kong et al. estimated a 44 cm^{-1} energy difference between m = 0 and m = ±1, with a ∼ 0.5 cm^{-1} splitting of the m = ±1 levels[22].

For two non-interacting *ortho*-H_2 molecules occupying primary sites, the ninefold degenerate J = 1 pair states are crystal field split into six separate levels, as shown by the third column in Fig. 2 (the notation is defined in Table S2). To include $H_2\cdots H_2$ interactions we build on the work with solid hydrogen. Because the J = 0 rotational state has no quadrupole moment both *para*-$H_2\cdots$*para*-H_2, and *para*-$H_2\cdots$*ortho*-H_2 interactions are negligible in comparison to those of *ortho*-$H_2\cdots$*ortho*-H_2[1]. Thus we can restrict our analysis to *ortho*-H_2, which for the temperatures used in this study are in the J =1 rotational state. For two isolated J = 1 molecules their interaction is dominated by the EQQ term that scales with R^{-5}. The EQQ coupling constant, $\Gamma(R)$ has a value in solid hydrogen of 0.56 cm^{-1} for a nearest-neighbor distance of 3.8 Å[1]. In the case of MOF-5, where the nearest-neighbor sites are 6.2 Å apart, we would expect Γ to be 0.06 cm^{-1}. The EQQ interaction potential is given by[1]

$$\Phi_{EQQ}(R_{12}) = 4\pi\frac{5}{6}\sqrt{70}\Gamma(R_{12})\sum_{\mu} C(224;\mu,-\mu) \times Y_2^{\mu}(\omega_1)Y_2^{-\mu}(\omega_2), \quad (1)$$

where R_{12} is the $H_2\cdots H_2$ separation distance, ω_i are the polar angles of the respective H_2 molecules with regards to a Z_{12}-axis (see Fig. 1) joining their centers, $C(224;\mu,-\mu)$ is a Clebsch-Gordon coefficient, and $Y_2^{\mu}(\omega_i)$ a spherical harmonic.

To represent the EQQ effect in the crystal frame rather than the vector joining the molecular centers we follow the approach of Gray, which leads to[25]

$$\Phi_{EQQ'}(R_{12}) = \frac{20\pi}{9}\sqrt{70\pi}\Gamma(R_{12})\sum_{M,N} C(224;MN) \times Y_2^{M}(\Omega_1)Y_2^{N}(\Omega_2)Y_4^{M+N}(\Omega_{12})^*, \quad (2)$$

where Ω_i are the polar angles of the respective molecule in the crystal frame and Ω_{12} is the angle between the Z_1 and Z_{12} axes. The fourth column in Fig. 2 shows the resulting energy level scheme in which both the crystal field and EQQ terms are included. The ninefold degeneracy is now completely lifted, with four levels grouped at lower energy and five more at much higher. The five upper levels correspond to the case where at least one of the H_2 molecules has m = 0 in either the Z_1 or Z_2 frame. The lower four levels are linear combinations of m = ± 1 in their own frame. For the temperatures used in this study only the four lower energy levels are thermally populated.

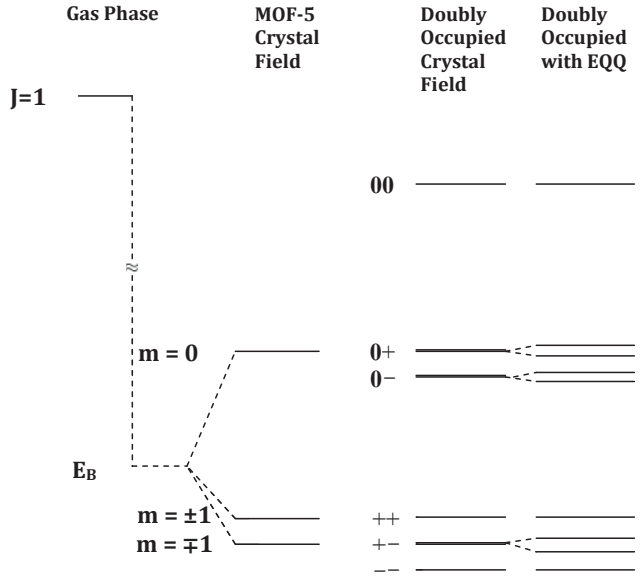

FIG. 2: Energy diagram for the J = 1 level of H_2 at the primary site in MOF-5. The first column shows an isolated J = 1 molecule, the second a single J = 1 molecule in MOF-5 with binding energy E_B, the third two non-interacting H_2 molecules in MOF-5, and the fourth two J = 1 molecules interacting via the EQQ potential in MOF-5.

III. EXPERIMENTAL PROCEDURE

The synthesis and characterization of the MOF-5 samples used in this paper have been presented in our previous report[21]. Infrared measurements were taken using a Bomem DA3 spectrometer with both quartz halogen and globar sources, in conjunction with a KBr beamsplitter and mercury cadmium telluride and indium gallium arsenide detectors. A broadband visible filter was used to minimize sample heating by the IR source. In all cases measurements were performed using the diffuse reflectance technique outlined in our earlier work[20]. This technique significantly enhances the IR signal of adsorbed H_2 in comparison to traditional transmission measurements. A custom-built cryogenic chamber allows the sample powders to be mounted, degassed, cooled, and dosed with hydrogen without exposing them to air[26]. Dosing with *normal*-H_2 (H_2 with a 3:1 *ortho:para* ratio) is performed at 77 K using a Micromeritics ASAP 2020 instrument. The sample is then cooled to the system's base temperature of 15 K at a rate of 5 K/minute. This rate is chosen as the optimal to achieve thermal equilibrium while minimizing *ortho* to *para* conversion within the MOF. The overall pressure drop is used to determine the quantity of gas adsorbed. In all cases spectra are referenced to the background spectrum of MOF-5 containing only He thermal exchange gas.

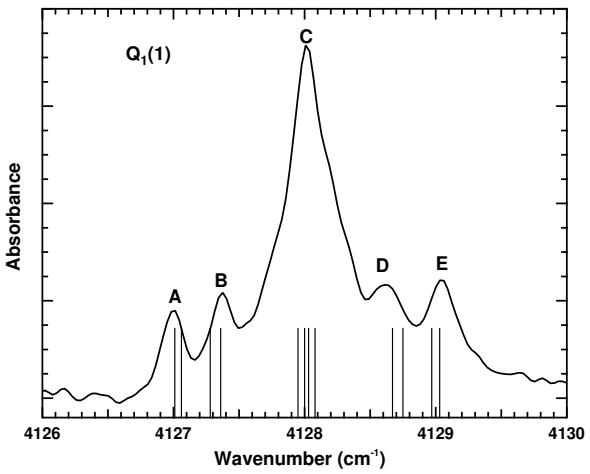

FIG. 3: Infrared absorption spectrum at 15 K showing the $Q_1(1)$ transition for a concentration of 2 H_2 per MOF cluster. The instrument resolution is 0.1 cm^{-1}. The stick spectrum is based on an m = ± 1 splitting of 0.8 cm^{-1} and a Γ value of 0.06 cm^{-1}.

IV. RESULTS AND DISCUSSION

A. Fine structure spectrum

Due to the well known vibrational-rotational coupling, the vibrational spectrum of gas phase H_2 contains $Q_1(1)$ and $Q_1(0)$ modes separated by 6 cm^{-1}[27] (the number in parentheses refers to the J value and the subscript 1 indicates a transition to the $\nu = 1$ vibrational state). In the case of H_2 in MOF-5 the separation is increased to 8 cm^{-1} with the $Q_1(1)$ mode at 4128 cm^{-1} and $Q_1(0)$ at 4136 cm^{-1}[20,21]. The identification of these peaks as $Q_1(1)$ and $Q_1(0)$ is confirmed by their *ortho* to *para* conversion over time. Figure 3 shows the IR absorption spectrum at 15 K in the $Q_1(1)$ region for a concentration of two H_2 per MOF cluster. The $Q_1(1)$ band is composed of at least five distinct peaks while in contrast the $Q_1(0)$ (see Fig. S1 supplemental material[28]) band appears with a single distinct peak. The $Q_1(1)$ sidebands, labeled A, E and B, D are almost symmetrically displaced to the low and high frequency side from the central band, C. The C band is somewhat broader than the sidebands A, B, D, and E, with the $Q_1(0)$ having a significantly smaller FWHM than any of the $Q_1(1)$ bands. As shown in Fig. S2, the sidebands broaden significantly with increasing temperature such that individual FS features are no longer apparent at 25 K[28].

B. Concentration Dependence

Figure 4 shows the absorption spectra for a series of increasing H_2 concentrations. The concentrations listed are based on the total adsorbed quantity of H_2 as determined by the pressure drop upon loading. For *normal*-H_2

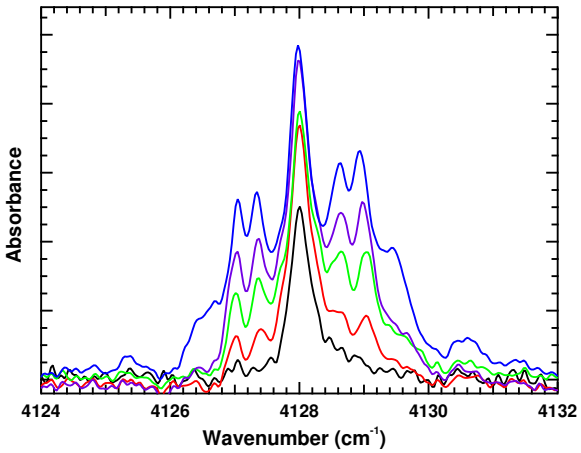

FIG. 4: (Color online) Infrared absorption spectra at 15 K showing the $Q_1(1)$ transition for H_2 concentrations of 0.7 (black), 1.3 (red), 2.0 (green), 2.7 (purple), and 4 (blue) H_2 per MOF cluster. The instrument resolution is 0.1 cm^{-1} for all spectra.

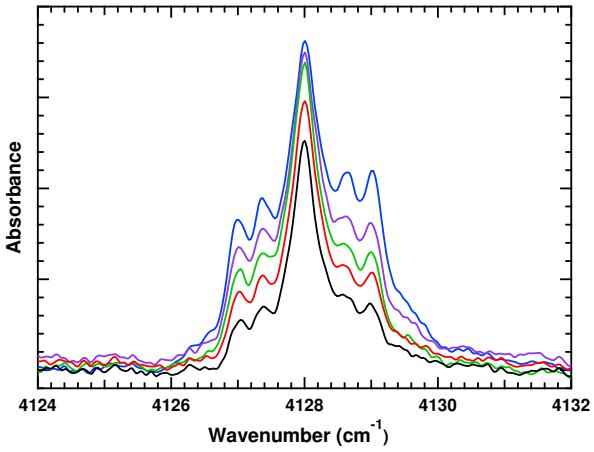

FIG. 5: (Color online) Infrared absorption spectra at 15 K for a concentration of 2.9 H_2 per MOF cluster at times of 40 (blue), 100 (purple), 130 (green), 190 (red), and 270 (black) minutes after H_2 was first introduced into the sample chamber at 77 K. The spectra show *ortho* to *para* conversion with time.

the *ortho* concentration is 3/4 of this value, but *ortho* to *para* conversion within the MOF may make the actual *ortho*-H_2 concentration slightly lower (see Fig. 5). At the lowest concentration of 0.7 H_2 ($\sim$ 0.5 *ortho*-H_2) per MOF cluster the spectrum is dominated by the central C band with only weak broad wings on either side. At a concentration of 1.3 H_2 ($\sim$ 1.0 *ortho*-H_2) per cluster the FS features are evident with indication that the D band is composed of at least two peaks. The sidebands become more pronounced with further increase in concentration and at the highest concentration shown in Fig. 4 there are clearly new features outside of the five labeled in Fig. 3. In general the concentration dependence of bands A, B, D, and E are the same as each other and it seems likely that they have a common origin. As shown in Fig. S3 the intensity of these FS bands relative to that of the central C band initially increases nearly linearly with concentration before curving over at higher concentration.

In addition to enabling the characterization of peaks as *ortho* or *para*, the evolution of the spectra with time provide further evidence to the origin of the FS bands. Figure 5 shows the $Q_1(1)$ absorption spectra over a time period from 40 to 270 minutes after loading. All of the peaks decrease in intensity with time, indicating that they originate from *ortho*-H_2. The central C band's time dependence is similar to that of the main rovibrational $S_1(1)$ band (see Fig. S4[28]). However, the FS bands show a much more dramatic decrease consistent with an origin from *ortho*-H_2 pairs or higher number groups. In many ways the time dependence of the $Q_1(1)$ FS is similar to that of the concentration dependence, indicating that the behavior arises from a changing *ortho*-H_2 concentration at a particular crystallographic site rather than the occupancy of some new MOF environment.

The fact that the FS is only present for the *ortho* $Q_1(1)$ mode, that it appears under conditions when only the primary site should be occupied, that the relative intensity of the FS grows with increasing concentration, and that it decreases with *ortho* to *para* conversion over time all point to the bands A, B, D, and E arising from pairs of interacting H_2 molecules. In the case of solid hydrogen, interacting H_2 pairs lead to so called double transitions[29,30]. These are ones in which two molecules are excited by a single photon and arise through the quadrupole field of one H_2 inducing a dipole moment via the polarizability of a second H_2[3,5,6]. In addition to producing FS in both $Q_1(1)$ and $Q_1(0)$ modes, double transitions also lead to additional bands associated with rovibrational S-transitions[5,10,31]. We see no evidence for these double transitions which is not surprising given the large $H_2 \cdots H_2$ separation in MOF-5. An estimate of the double transition intensity, which is proportional to $(Q\alpha R^{-4})^2$, where Q is the H_2 quadrupole moment, α its polarizability, and R the nearest neighbor separation, is more than two orders of magnitude less than estimates for single $H_2 \cdots$MOF-5 induced transitions[22]. It thus seems unlikely that the observed FS features arise from double transitions.

Restricting our analysis to single transitions, i.e. ones in which only one H_2 molecule changes its quantum state, Fig. S5 shows the possible $Q_1(1)$ transitions in the frequency region around 4128 cm^{-1}[28]. These are grouped together in five distinct bands illustrated by the stick spectrum in Fig. 3. Due to the slight increase in the H_2 polarizability[32] and quadrupole moment[33] in its vibrationally excited state, these five bands are composed of 12 distinct transition energies. There are three parameters determining the structure of the stick spectrum. The first is the shift of the vibrationally excited J = 1 level relative to that of gas phase H_2. This is set to agree with

previous published experimental data[21] and is consistent with the empirically established relationship between the H_2 vibrational redshift and site binding energy[24,34,35]. The second parameter is the crystal field splitting of the m = ±1 levels for an isolated H_2 in MOF-5. A value of 0.8 cm^{-1} leads to good agreement with the data in Fig. 3. This value is 1.6 times greater than the 0.5 cm^{-1} estimated by Kong et al[22]. Similarly, the previously observed experimental value for the m = ±1 to m = 0 splitting is 1.4 times greater than the Kong theoretical estimate[22]. The final parameter controlling the stick spectrum is the Γ value for the EQQ interaction, which is set to be simply the distance scaled value based on that of solid H_2. By varying these three parameters we see that the shift controls the location of the central four lines that agree well with the C band frequency, the crystal field splitting controls separation of the side lines from the central group, while the Γ value for EQQ leads to the splitting between the two pairs on the high and low frequency side of the central group.

The experimental spectra indicate that the $H_2 \cdots H_2$ interaction in MOF-5 is somewhat stronger than that predicted by the simple EQQ interaction. The best fit (see Fig. S6[28]) indicates an EQQ interaction ∼ 15% greater than the scaled value based on solid H_2. This increased interaction could occur from H_2 modification by the MOF-5, either through polarization or charge-transfer[15]. Also, our model is very simple and does not include center-of-mass translational state averaging or effects due to triply and quadruply occupied MOF clusters. Finally, we note that the presence of the four central lines in the stick spectrum, indicates a contribution to the C band intensity from both single and pairs of *ortho*-H_2. This explains the curving over of the relative intensity plot at higher concentration in Fig. S3.

For the concentration range shown in Fig. 4 there are no additional features associated with the $Q_1(0)$ mode or at the known location of bands arising from secondary site occupancy[20]. This is consistent with neutron diffraction data, which indicate that under our loading conditions the binding energy difference between the primary and secondary sites is such that at equilibrium essentially all of the adsorbed H_2 populates the primary site with no significant occupancy in secondary sites[19]. The additional features appearing in the highest concentration spectra in Fig. 4 are most likely the result of triply or quadruply occupied MOF clusters. Modeling the spectrum of such J = 1 clusters is beyond the scope of this paper and even in the much simpler case of solid hydrogen has rarely been done[3,5]. The $H_2 \cdots H_2$ interaction energy (< 0.1 meV) is too small to produce any significant grouping of the adsorbed H_2 at the primary sites above and beyond a simple random distribution[28].

An interesting aspect of the spectra shown in Fig. 4 is the lack of FS sidebands at the lowest concentration when most of the adsorbed H_2 are in singly occupied clusters. Even in the absence of $H_2 \cdots H_2$ interactions, crystal-filed effects from the MOF leads to a ∼ 0.8 cm^{-1} splitting between m = ± 1 levels. This could lead to FS bands at ± 0.8 cm^{-1} on either side of the central C band[28]. Their presence depends on whether $\Delta m = \pm 2$ transitions are allowed for singly occupied clusters. Theoretical calculations of Kong et al. predict a large dipole moment associated with such transitions[22]. We do not observe any corresponding features in the spectra. While it is possible that the bands are present but with too low an intensity to be observed, it appears that the experimental data and theoretical predictions are inconsistent with each other in this aspect.

C. D_2 Addition

As a final test to establish the origin of the FS features, we examined the behavior of an H_2/D_2 mixture. Because the fundamental vibrational frequency of D_2 is $\sim 1/\sqrt{2}$ that of H_2, its presence should not produce any direct features in the H_2 spectral region[27]. This is confirmed by loading the MOF-5 sample with D_2. However, D_2 has a very similar quadrupole moment to H_2 (reduced by 1.6 %)[1] and thus it should enhance any H_2 features arising from an EQQ interaction. The black curve in Fig. 6 shows the spectrum for 0.7 H_2 per MOF cluster while the red curve shows that for the same concentration of H_2 but with an additional 2.7 D_2 per cluster. The addition of the D_2 results in only minor changes to the $Q_1(0)$ and central $Q_1(1)$ C bands but a dramatic increase in the $Q_1(1)$ FS. This strongly supports the idea that the H_2 FS originates from EQQ interactions. Given the small difference in quadrupole moments between H_2 and D_2 we would not expect to see any noticeable change in the frequency of the FS peaks upon D_2 addition.

Due to the presence of overlapping MOF-5 bands it is impossible to resolve the fundamental D_2 $Q_1(1)$ bands in the range of 2990-2995 cm^{-1}. While the overtone bands are clearly visible, we see almost no sign of FS for either D_2 or H_2 (see Fig. S8[28]). This is consistent with earlier findings that in the overtone region IR activity arising through H_2 polarization is significantly enhanced relative to that based on the H_2 quadrupole moment[21]. The H_2 polarizability tensor is dominated by the isotropic term, which does not contribute to transitions with $\Delta m \neq 0$[36] and hence does not lead to any FS bands.

V. SUMMARY

In summary, low temperature spectra reveal a mostly symmetric FS for the $Q_1(1)$ band of H_2 in MOF-5. The concentration dependence, time dependence revealing *ortho* to *para* conversion, and response to D_2 addition all indicate a FS arising from *ortho*-H_2 $\cdots$ *ortho*-H_2 interactions. The observed peak splitting is explained well through EQQ interactions of multiple H_2 molecules in conjunction with crystal field effects from the MOF-5 cluster. As expected, this relatively simple model does

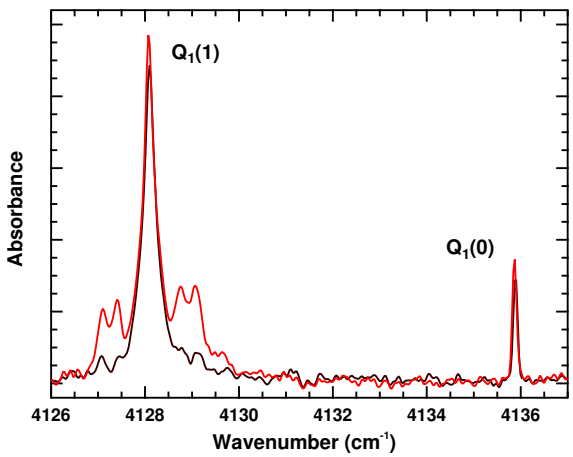

FIG. 6: (Color online) Infrared absorption spectra at 15 K for a concentration of 0.7 H_2 per MOF cluster (black) and a mixture of 0.7 H_2 and 2.7 D_2 per MOF cluster (red). The instrument resolution is 0.1 cm^{-1}.

not capture all of the spectral features. Most notably it does not explain the additional substructure to the C and D bands nor the slight asymmetry in intensity and frequency between the high and low frequency sidebands. Most interestingly, the splitting of the FS peaks is somewhat greater than predictions based on unmodified $H_2 \cdots H_2$ interactions. This is consistent with recent work that suggests that even for weakly bound H_2 a significant degree of charge-transfer and H_2 polarization occurs[15]. Future work will look to incorporate these modifications and examine the FS behavior of adsorbed H_2 in more strongly binding MOFs where the $H_2 \cdots H_2$ interactions should deviate more dramatically from that of solid hydrogen.

ACKNOWLEDGMENTS

This work was supported by an award from the NSF, grant # CHE-1111896. We thank Corina Miner and Hanna Pieper for their help with data acquisition and Kinori Rosnow for his help with the manuscript preparation. We are saddened to report the untimely death of Jesse Rowsell during the writing of this manuscript.

* Electronic address: sfgerald@oberlin.edu

1. I. F. Silvera, Rev. Mod. Phys. **52**, 393 (1980).
2. J. Van Kranendonk, *Solid Hydrogen* (Plenum, New York, 1983).
3. J. Sears, V.F.and Van Krenendonk, Can. J. Phys. **42**, 980 (1964).
4. M. Chan, M. Okumura, C. Garbys, L. Xu, B. Rehfuss, and T. Oka, Phys. Rev. Lett. **66**, 2060 (1991).
5. M. Mengel, B. Winnewisser, and M. Winnewisser, J. Mol. Spect. **188**, 221 (1998).
6. Y. Zhang, T. Byers, M. Chan, T. Momose, K. Kerr, D. Weliky, and T. Oka, Phys. Rev. B **58**, 218 (1998).
7. K. Yoshioka, P. L. Raston, and D. T. Anderson, Int. Rev. Phys. Chem. **25**, 469 (2006).
8. W. Hardy, A. Berlinsky, and A. Harris, Can. J. Phys. **55**, 1150 (1977).
9. W. Mengel, B. P. Winnewisser, and M. Winnewisser, Phys. Phys. B **55**, 10420 (1997).
10. A. Mishra, R. D'Souza, and T. Balasubramanian, Phys. Rev. B **70**, 174303 (2004).
11. M. Schroder, ed., *Functional Metal-Organic Frameworks: Gas Storage, Separation and Catalysis, Topics in Current Chemistry, 293* (Springer, 2010).
12. L. R. MacGillivray, ed., *Metal-organic frameworks: design and application* (Wiley, 2010).
13. D. Farrusseng, ed., *Metal-organic frameworks: applications from catalysis to gas storage* (Wiley-VCH, 2011).
14. H.-C. Zhou and S. Kitagawa, Chem. Soc. Rev. **43**, 5415 (2014), and other articles in the themed collection.
15. E. Tsivion, J. R. Long, and M. Head-Gordon, J. Am. Chem. Soc. **136**, 17827 (2014).
16. S. Keskin, J. Liu, R. B. Rankin, J. K. Johnson, and D. S. Sholl, Ind. & Eng. Chem. Res. **48**, 2355 (2009).
17. S. S. Kaye, A. Dailly, O. M. Yaghi, and J. R. Long, J. Am. Chem. Soc. **129**, 14176 (2007).
18. T. Yildirim and M. R. Hartman, Phys. Rev. Lett. **95**, 215504 (2005).
19. E. C. Spencer, J. A. K. Howard, G. J. McIntyre, J. L. C. Rowsell, and O. M. Yaghi, Chem. Commun. **3**, 278 (2006).
20. S. A. FitzGerald, K. Allen, P. Landerman, J. Hopkins, J. Matters, R. Myers, and J. L. C. Rowsell, Phys. Rev. B **77**, 224301 (2008).
21. S. A. FitzGerald, J. N. Nelson, E. Gilmour, and J. L. C. Rowsell, J. Mol. Spect. **307**, 20 (2015).
22. L. Kong, Y. J. Chabal, and D. C. Langreth, Phys. Rev. B **83**, 121402 (2011).
23. I. Matanovic, J. L. Belof, B. Space, K. Sillar, J. Sauer, J. Eckert, and Z. Bacic, J. Chem. Phys. **137**, 014701 (2012).
24. S. Bordiga, J. G. Vitillo, G. Ricchiardi, L. Regli, D. Cocina, A. Zecchina, B. Arstad, M. Bjorgen, J. Hafizovic, and K. P. Lillerud, J. Phys. Chem. B **109**, 18237 (2005).
25. C. Gray, Can. J. Phys. **46**, 135 (1968).
26. S. A. FitzGerald, H. O. H. Churchill, P. M. Korngut, C. B. Simmons, and Y. E. Strangas, Rev. Sci. Inst. **77**, 4 (2006).
27. B. P. Stoicheff, Can. J. Phys. **35**, 730 (1957).
28. See supplemental material at...
29. T. Balasubramanian, R. D'Souza, R. D'Cunha, and K. Rao, J. Mol. Spec. **153**, 741 (1992).
30. A. Mishra, R. D'Souza, and T. Balasubramanian, J. Mol. Spec. **235**, 206 (2006).
31. S. N. Yurchenko, B. Assfour, E. V. Lavrov, and G. Seifert, Royal Soc. Chem. Adv. **2**, 9839 (2012).
32. W. Kolos and Wolniewicz.L, J. Chem. Phys. **46**, 1426 (1967).
33. G. Karl and J. D. Poll, J. Chem. Phys. **46**, 2944 (1967).
34. C. O. Areán, S. Chavan, C. P. Cabello, E. Garrone, and G. T. Palomino, Chem. Phys. Chem. **11**, 3237 (2010).

[35] S. A. FitzGerald, B. Burkholder, M. Friedman, J. B. Hopkins, C. J. Pierce, J. M. Schloss, B. Thompson, and J. L. C. Rowsell, J. Am. Chem. Soc. **133**, 20310 (2011).

[36] H. P. Gush, W. F. Hare, E. Allen, and H. L. Welsh, Can. J. Phys. **38**, 176 (1960).